Liquid Crystals
Publication details, including instructions for authors and subscription information:
http://www.informaworld.com/smpp/title~content=t713926090

Strain-induced compression of smectic layers in free-standing liquid crystalline elastomer films

V. Aksenov[a]; J. Bläsing[a]; R. Stannarius[a]; M. Rössle[b]; R. Zentel[b]
[a] Otto-von-Guericke-Universität Magdeburg, Institut für Experimentelle Physik, D-39106 Magdeburg [b] Universität Mainz, Inst. für Organische Chemie, D-55099 Mainz, Germany

To cite this Article Aksenov, V. , Bläsing, J. , Stannarius, R. , Rössle, M. and Zentel, R.(2005) 'Strain-induced compression of smectic layers in free-standing liquid crystalline elastomer films', Liquid Crystals, 32: 7, 805 — 813
To link to this Article: DOI: 10.1080/02678290500161363
URL: http://dx.doi.org/10.1080/02678290500161363

Liquid Crystals, Vol. 32, No. 7, July 2005, 805–813

Taylor & Francis
Taylor & Francis Group

Strain-induced compression of smectic layers in free-standing liquid crystalline elastomer films

V. AKSENOV*†, J. BLÄSING†, R. STANNARIUS†, M. RÖSSLE‡ and R. ZENTEL‡

†Otto-von-Guericke-Universität Magdeburg, Institut für Experimentelle Physik, Universitätsplatz 2, D-39106 Magdeburg

‡Universität Mainz, Inst. für Organische Chemie, Duesbergweg 10–14, D-55099 Mainz, Germany

(*Received 7 February 2005; accepted 11 April 2005*)

The deformation of oriented smectic liquid crystal elastomer films with smectic layers parallel to the film surface was studied using optical reflectometry and small angle X-ray diffraction. Reflectometry data show that in the chosen material, in-plane strain causes a change in the optical thickness of the free-standing films. Small angle X-ray scattering was used to explore the molecular origin of this effect. The X-ray scattering data confirm that the change in optical thickness originates from the compression of the individual smectic layers. The measured Poisson ratio in the smectic A and C* phases is close to ½, in contrast to the smectic elastomers investigated earlier by Nishikawa et. al. [*Macromol. Chem. Phys.* **200**, 312 (1999)]. In this unique material, the molecular lattice dimensions can be reversibly controlled by macroscopic stretching of the oriented samples.

1. Introduction

The unique properties of liquid crystal elastomers (LCEs), combining rubber elasticity and anisotropic liquid crystal properties, have made them objects of intensive investigation in recent years [1–31]. The polymer network couples the orientation of the mesogenic subunits with the mechanical deformations of the material, but only slightly affects the liquid crystalline phase transitions. Due to the coupling of macroscopic and microscopic properties, such as the interactions between sample shapes and dimensions and the orientation of the mesogenic units, LCEs are promising candidates for diverse technological applications. For example, the change of the director orientation pattern on the application of external electric fields [1, 2] or a thermally induced change of the order parameter during phase transitions [3] may lead to macroscopic sample deformations.

The mechanical properties of LCEs are in general different from those of conventional isotropic rubbers. Deformations in the plane of the smectic layers are governed by the entropy elasticity of the polymer chains, as in a two-dimensional isotropic rubber network, and the elastic moduli are expected to be in the order of $\mu_t \sim nkT$; as in conventional isotropic rubbers. In the case of deformations perpendicular to the smectic layers, the elastic response includes enthalpic terms with a modulus μ_n usually much larger than the modulus of entropy elasticity of an isotropic rubber [4, 5] and comparable to the smectic layer compression constant. Experimentally, very different moduli have been reported for deformations of oriented (single crystal) smectic LCE strips parallel and perpendicular to the smectic layers in the smectic A (SmA) phase, they differ by two orders of magnitude [4, 5].

One may expect that, under these conditions, the uniaxial stretching of the material in the smectic layer plane will not change the extension of the sample perpendicular to the layers but the strain will be compensated by a compression in the layer plane, perpendicular to the stretching direction. For SmA LCEs under uniaxial stress in the plane of the smectic layers, a Poisson ratio close to 1 in the smectic layer plane, and zero perpendicular to it, has been reported [5]. The Poisson ratio ν of an isotropic material is the ratio of the transverse contraction strain and the longitudinal extension strain in the stress direction, $\nu = -\varepsilon_t/\varepsilon_l$, where the strain is defined as the relative length change $\varepsilon = \Delta l/l_0$.

For the material investigated in this work, we found earlier that during the stretching of free-standing films with the smectic layers parallel to the film surface, the optical thickness of the sample changes and the measured Poisson ration is close to ½, as in an isotropic

*Corresponding author.
Email: victor.aksenov@physik.uni-magdeburg.de

Liquid Crystals
ISSN 0267-8292 print/ISSN 1366-5855 online © 2005 Taylor & Francis
http://www.tandf.co.uk/journals
DOI: 10.1080/02678290500161363

rubber [6]. There are different possible explanations of such behaviour. The first is that some smectic layers break during stretching and the lateral extension is compensated by a reduction of the number of smectic layers, leading to a decreasing film thickness. But even at strains up to more than 50 %, the deformation of the film and the related film thickness changes are almost completely reversible. This contradicts such a simple explanation.

The second hypothesis is that strain induces a tilt of the mesogenic units in the SmA phase or increases the tilt angle in the smectic C* phase. If a mesogenic tilt is induced by lateral strain in an ordinary SmA phase, it is reasonable to assume that its azimuth is defined by the stretching axis, with the consequence of a large induced in-plane birefringence of the film. This is in contrast with experimental observations. Moreover, the induced tilt mechanism is ineffective for very small tilt angles. Since the linear dependence of the layer compression on tilt angle variations vanishes at zero tilt, one would expect a pronounced non-linear behaviour in that case. Neither argument is applicable if one deals with a so-called de Vries smectic A phase, which has been suggested earlier [32], and we discuss this scenario in more detail later. An alternative explanation is the mutual penetration of the smectic layers, or other mechanisms leading to actual compression of the smectic layers. So far, there has been no direct evidence for or against such a mechanism in smectic elastomers.

The goal of this work is to study the deformations of thin oriented LCEs films using X-ray spectroscopy and optical reflectometry, and to explore the relation between the optically observed thickness changes of the film (macroscopic effect) and smectic layer compression (as its possible microscopic origin). The question we are trying to answer is: do the observed optical thickness changes correspond to actual film thickness changes, and particularly to changes of the individual smectic layer spacings? X-ray measurements allow us to determine the thickness of smectic layers under the influences of lateral strain and to clarify this question. Moreover, we seek structural differences between the behaviours of elastomers films in the SmA and SmC* phases.

2. Experimental

The material used to prepare free-standing films was a random side chain copolymer, with the chemical structure shown in figure 1. It consists of a siloxane backbone with non-substituted, mesogen-substituted and crosslinker- substituted segments in the ratios 2.7:0.95:0.05. The crosslinker units have a structure and length similar to the mesogenic substituents, except for a terminal photoreactive group.

In the material chosen, crosslinks are formed between different siloxane sublayers (interlayer crosslinking). As a result, the material forms a 3D network, and the coupling between the orientation of the mesogens and the polymer network is strong in comparison with so-called intralayer crosslinked elastomers, in which crosslinks are formed preferentially within the siloxane sublayers [7].

The phase sequence in the non-crosslinked material is SmX 65°C SmC* 95–96°C SmA 125°C I. Samples for the X-ray measurements were prepared by irradiation of free-standing films of the photo-crosslinkable polymer (in the SmA phase) using a 250 W Panacol-Elosol UV point source UV-P 280. The geometry used for film preparation is shown in figure 2.

During UV crosslinking, two side edges of the free standing film are shielded from UV exposure with an opaque mask [1]. After crosslinking, the sample consists of an elastomer strip in the middle and two liquid parts at both sides of this strip; these liquid edges can be easily removed. This method allows us to obtain free-standing films fixed at two opposite edges [1, 6]. The UV irradiation time was 2 h; it was performed in two

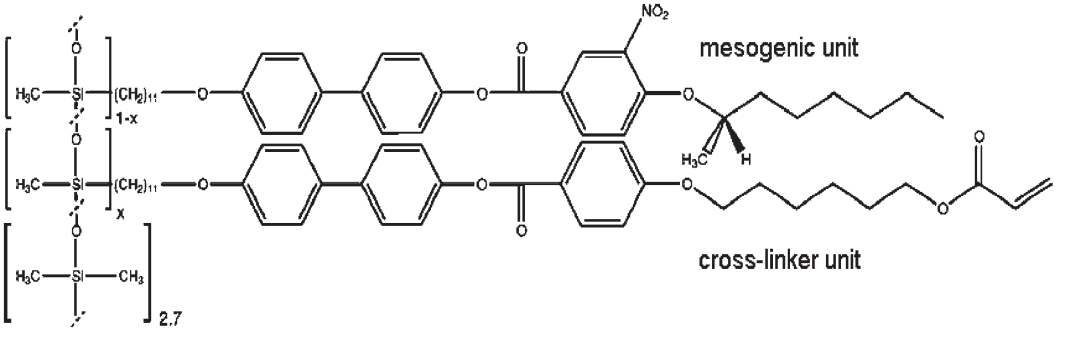

Figure 1. Chemical composition of the precursor copolymer, a three-kernel material with crosslinker fraction $x = 0.05$.

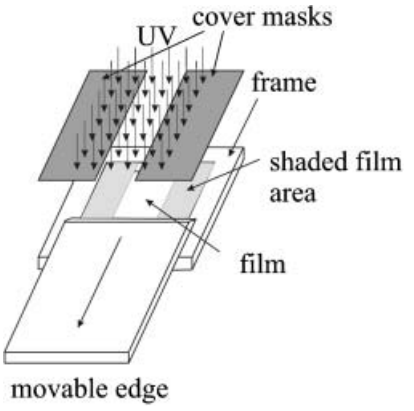

Figure 2. Schematic diagram of the film preparation set-up.

steps. In the first step, the sample was irradiated for 1 h with the mask; in the second step, it was irradiated for 1 h without the mask, after the liquid parts at the sides of the film had been removed. The minimum required exposure time for complete crosslinking of the film has not been established and, it may be sufficient to irradiate the sample for a much shorter time. After UV irradiation, the sample consists of a well oriented free-standing film with an area of approximately 5 mm^2 and a thickness of approximately 0.5 μm. Most of the smectic material, however, is contained in the lateral meniscus of the film which extends over a region of a few dozen micrometers from the edges of the support, and in the bulk material on the support itself, see both sides of figure 3 (*a*). The thickness of the meniscus can be much larger than the film thickness, and in contrast to the film, the smectic layers may be randomly oriented in the meniscus and the bulk phase.

Small angle X-ray scattering (SAXS) and optical reflectometry methods were used to explore the deformations of the single crystal LCE films. The SAXS measurement set-up consists of a goniometer URD 6 and an X-ray generator ID 3000 (Seifert/FPM) with a copper fine focus tube (line focus 40 mm × 8 mm) at 35 kV/15 mA. A primary plane-crystal monochromator Ge(1 1 1) and a 60 mm divergence slit in front of the sample heater provide $CuK_{\alpha 1}$ radiation ($\lambda = 0.15406$ nm) with a resolution of 0.01° (Θ). The scattered and reflected intensities (including air and slit scattering) were measured with a position sensitive detector PSD 50M (Braun) using a resolution of 0.012° (2Θ). For the estimation of relative smectic layer thickness variations, the evaluation of the peak positions with the help of Braggs law $d = \lambda/(2 \sin \Theta)$ is sufficient. During the X-ray measurements, the sample assembly was placed in a copper heating box for temperature control.

The optical reflectometry method exploits the interference between the beam reflected at the top surface of the free-standing film and the beam reflected at the bottom surface of the film [6]. If the thickness of the film is of the order of a few wavelengths of visible light, the reflection image of the film in white light appears coloured and the interference colour gives a good estimate of the film thickness. White light and monochromatic ($\lambda = 547$ nm) reflection images were used for the determination of the film thickness. Colour images allow us to define the correct order of interference and the monochromatic images allow a quantitative calculation of the optical phase difference $\Delta\varphi$. The film reflectivity is

$$R(\lambda) = \frac{4\rho^2 \Big/ (1-\rho^2)^2 \sin^2 \Delta\varphi}{1 + 4\rho^2 \Big/ (1-\rho^2)^2 \sin^2 \Delta\varphi},$$
$$\text{with } \Delta\varphi = 2\pi n_0 \frac{d_{\text{film}}}{\lambda} \text{ and } \rho = \frac{n_0 - 1}{n_0 + 1}. \quad (1)$$

For small values of ρ one can use an approximate formula:

$$R(\lambda) = 4\rho^2 \Big/ (1-\rho^2)^2 \sin^2 \Delta\varphi \quad (2)$$

where d is the film thickness, λ is the wavelength and n_0 is the effective refractive index, which corresponds to the ordinary refractive index in the smectic A phase. Using this approximation and the experimental reflectivity dependence, the phase difference for any point of the film can be found. Knowing this phase difference, one can determine the optical path $2\pi d_{(opt)}/\lambda = \Delta\varphi$ and the film thickness $d_{\text{film}} = d_{(\text{opt})}/n_0$. Since the refractive index is not known exactly, we use the approximate value $n_0 = 1.5$ for thickness calculations. The error in the calculation of $\Delta\varphi$ results from the experimental error in the measurement of the reflectivity at a given wavelength. Because $R(\Delta\varphi)$ at fixed wavelength is not linear but proportional to $\sin^2(\Delta\varphi)$, the experimental uncertainty also depends on the position on the reflectivity curve: the uncertainty is largest close to maxima and minima of the reflectivity curve, and smallest where $R = 1/2\ R_{\max}$. The film thickness can be evaluated with an accuracy of ± 35 nm close to maxima and minima of the reflectivity function, and ± 20 nm where the reflectivity is equal to ½ of the maximum value.

3. Results

3.1. *Optics*

The influence of strain on the thickness of free-standing LCE films crosslinked in the SmA phase was first

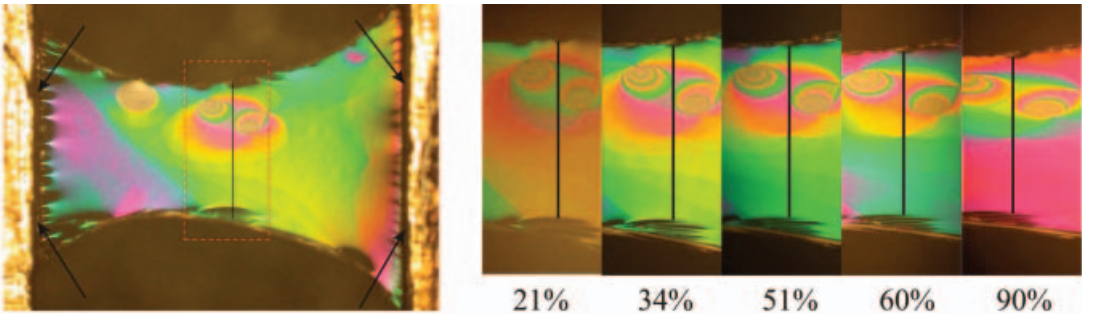

Figure 3. (*a*) Reflection image of the free-standing film of smectic LCE in white light; the film was crosslinked at $T = 120^{\circ}$C in the smectic A phase, $\varepsilon_x = 34\%$. The arrows point at the meniscus with non-oriented material. (*b*) Middle part of the film shown in figure 3 (*a*), at different strains, ε_x in % is given below the images.

studied by the optical reflectometry method [6]. We repeat here the experiments of [6] with slightly modified preparation conditions. The idea is to ensure that the optical and X-ray data are obtained from the same charge of material under identical preparation conditions. Figure 3 (*a*) shows the colour image of a free-standing LCE film with 34% lateral strain at $T = 120^{\circ}$C in the SmA phase. Figure 3 (*b*) is composed of images of the centre of the same film, at different strains. The interference colour change reflects the change of the optical thickness $d_{(\mathrm{opt})} = n_0 d_{\mathrm{film}}$, while the island topology (consisting of additional smectic layers) remains unchanged; the deformations are reversible. For quantitative film thickness measurements, monochromatic images at 547 nm illumination are evaluated. Positions of equal reflectivity, which mark regions of equal optical thickness, change in these images and provide evidence for optical thinning (decreasing $\Delta\varphi$) with increasing uniaxial strain.

Figure 4 (*a*) shows film thickness profiles calculated from the optical reflectivity for the given cross-section of the film shown in figure 3 at different values of deformation. The width y' of the film decreases during stretching—cf. figure 3 (*b*)—and the profiles in figure 4 (*a*) have been rescaled to the same reduced width. Figure 4 (*b*) shows for illustration the dependence of the film thickness upon strain (open and solid squares) at two given points on the film, labelled as positions 1 and 2 in the film thickness profiles of figure 4 (*a*). Here, we have tacitly assumed that the refractive index change during stretching is negligible, and have calculated the film thickness change from the change of the optical thickness by division by the refractive index n_0. This assumption needs to be verified

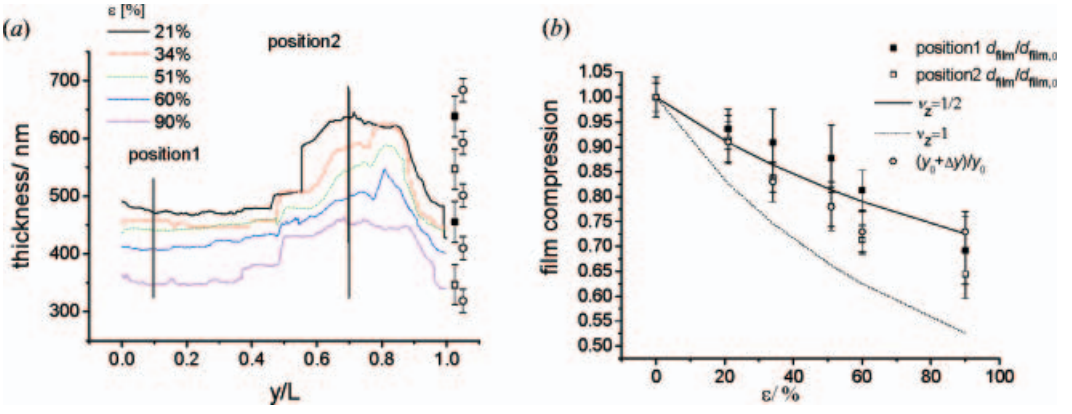

Figure 4. (*a*) Thickness profiles of a film calculated for a given cross-section from the optical reflectivity at wavelength $\lambda = 547$ nm. The width of the film depends on strain, and has been rescaled in the graph. L is the width of the film at a given deformation. Symbols ■ mark thicknesses for maximal reflectivity, □ mark reflectivity minima and ○ mark thicknesses for intermediate reflectivity, the corresponding error bars reflect the respective experimental uncertainty. (*b*) Normalized film thickness for two given points of the cross-sections as a function of deformation; $d_{\mathrm{film},0}$ is the thickness of the non-deformed film. The solid line represents the film thickness change expected for an isotropic material (Poisson ratio ½) and the dashed line gives the characteristics for a material with Poisson ratio $\nu = 1$ in the film plane. The reduced width of the film cross-section is given by open circles.

in independent experiments. One justification is in the observed lateral compression of the film, as discussed next.

In the LCE material, we can reasonably assume that the volume of the sample is conserved: $V = x_0y_0z_0 = x'y'z' = const$, and $x'y'z'/x_0y_0z_0 = 1$, where, x_0, y_0, z_0 represent the initial dimensions of some arbitrarily chosen volume along the respective axes, and $x' = x_0+\Delta x$, $y' = y_0+\Delta y$, $z' = z_0+\Delta z$ are the dimensions of the same volume element after deformation. The x-axis is parallel to the stretching direction and the z-axis is taken perpendicular to the film surface. In an isotropic material, $y'/y_0 = z'/z_0 = (x_0/x')^{\frac{1}{2}}$, and

$$1+\varepsilon_y = 1+\varepsilon_z = \left(\frac{1}{1+\varepsilon_x}\right)^{\frac{1}{2}} \qquad (3)$$

where $\varepsilon_x = \Delta x/x_0$, $\varepsilon_y = \Delta y/y_0$, and $\varepsilon_z = \Delta z/z_0$; Δx is the elongation in the direction of stress.

The solid line in graph 4(b) presents this theoretical thickness change of an isotropic, incompressible material with Poisson ratio ½, $\varepsilon_y = \varepsilon_z \approx (1-\varepsilon_x/2)^{\frac{1}{2}}-1$. For small deformations, it can be approximated by $\varepsilon_y = \varepsilon_z \approx -\varepsilon_x/2$. Since the lateral contraction of the film must compensate the product of strains in x and z, we have included in figure 4(*b*) the normalization factors $y'/y_0 = 1+\varepsilon_y$ for the widths of the film profiles, i.e. for the lateral in-plane extensions of the film near the middle between the drawing edges (dark bars in figure 3). In an isotropically deformed material, these points should coincide with the z'/z_0 data. From the graph, it can be seen that the optical thickness change indeed reflects the change of the film thickness, and the assumption of a constant n_0 is justified. The dashed line shows, for comparison, the lateral shrinkage in the film plane for a material with Poisson ratio 1 (no layer compression).

Errors in the determination of ε_x, ε_y, ε_z arise for the following reasons: the local strain along x is inhomogeneous in the film; we use as an approximation the separation of the two drawing edges. The actual strain ε_x at the position of the profiles in figure 3 may be somewhat larger (~10%) than the average strain, whereas it is smaller near the edges. The second source of error is the experimental accuracy in the determination of the y/y_0 of the order of $\pm 2\%$. The error of z/z_0 from the optical profiles, which has been discussed in the previous section, is ~7% close to maxima and minima of the reflectivity and reduces to ~4% where the reflectivity curve has its steepest slope.

The observed deformation characteristics are close to those of an isotropic rubber, and the Poisson ratio is close to ½. This is in contrast to other smectic A LCEs, studied by Nishikawa *et al.* [4, 5], and is incompatible with the assumption that the smectic layer compression moduli are much larger than the entropy elasticity moduli.

3.2. *SAXS*

X-ray measurements of the smectic layer spacing give an answer to the question of whether the film thickness change corresponds to an actual compression of individual smectic layers. A certain problem is the sensitivity of the available X-ray set-up, when the very small signal from the film is recorded. In previous work, the temperature dependence of the smectic layer spacing of the given material was studied using small angle X-ray scattering [8]. The measurements were performed on elastomer balloons, but in the balloon experiments it was impossible to measure the influence of strain on the smectic layer spacing. In the balloon geometry, strains of only a few percent could be achieved [8]. In this work, the compression of smectic layers has been studied in planar free-standing films. Figure 5 shows the experimental geometry for the SAXS diffraction measurements.

Measurements were performed at two different temperatures, $T = 90$ and 120°C, corresponding to the SmC* and SmA phases, respectively. The values of the smectic layer spacing obtained for the relaxed film at given temperatures are in a good agreement with those measured in the elastomer balloons [8]. Figure 6 shows SAXS data for the smectic elastomer film at zero deformation in the SmA phase. The intensity distribution for the non-stretched film has three peaks.

The lines labelled 1 and 3 correspond to the first and second order diffraction peaks of the bulk material, mainly located in the meniscus and on the metal frame, and only in small part from the signal of the free standing film. The second peak may correspond to some internal structure of the smectic layers with a characteristic length less than the smectic layer thickness. It is not

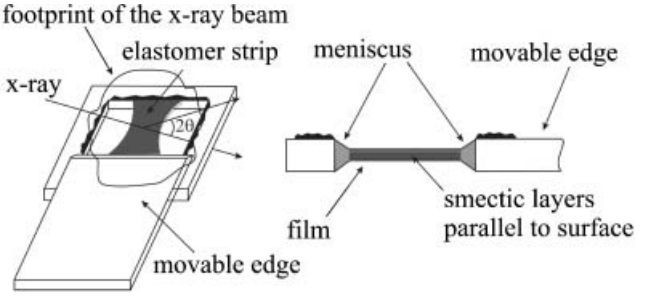

Figure 5. The geometry of the SAXS measurement for the free-standing smectic elastomer films.

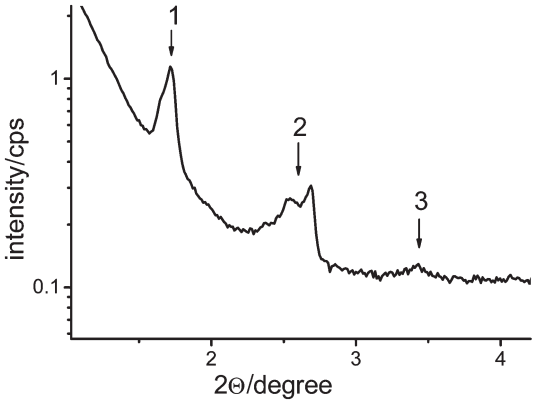

Figure 6. SAXS measurement for the free-standing smectic elastomer film at zero deformation in the SmA phase at $T = 120°C$.

relevant for this experiment and will not be discussed further.

The films were stretched under the microscope, and the optical thickness profile as well as strains in x and y were determined (see previous section). Samples were then placed in the SAXS set-up and the X-ray spectrum was recorded, before preparing the next deformation under the microscope. Thus, a sequence of optical and X-ray data was recorded. After the set of experiments, the drawing edges were moved again to their original positions, in order to verify the reversibility of the deformations. The strain was not completely reversible, a small residual deformation of a few percent remained when the samples had been stretched by more than 50%.

In the spectra of stretched films, a new X-ray scattering peak (1′) appears between the first and second peaks (figure 7). This peak corresponds to diffraction from the smectic layers in the thin film, which are stacked perfectly in the film plane. Initially, in the non-deformed film this peak is hidden in the bulk signal. The positions of the peaks corresponding to the bulk material do not change with the film deformation. Irrespective of the random orientation of the smectic layers in the meniscus and in the bulk material on the edges themselves, the Bragg condition is fulfilled at least for some part of the layers, and due to the large amount of bulk material compared with that in the free-standing film, the intensity of the X-ray peak originating from the bulk phase is higher than that from the oriented thin film.

The position of the small additional peak 1′ depends on the lateral strain. At zero strain of the film, the positions of peaks 1 and 1′ coincide. With increasing strain along x, the film peak 1′ shifts to larger diffraction angles, i.e. it reflects a decreasing lattice period. It would in some respect be preferable to measure the signal 1′ of the film alone, without the bulk signal, but this proves technically very difficult. In particular, the adjustment of the X-ray beam onto the film (which is contained in a sample holder consisting of the temperature controller and drawing frame) has to be repeated for every new film deformation; and the detection and adjustment of the small signal is extremely time consuming. Moreover, if the edges are covered by a mask, this also shields part of the thin film and decreases the intensity of the diffraction pattern. It proved to be more convenient to measure the X-ray scattering signal with a larger beam aperture and to ignore the bulk signal in the evaluation. Most experiments have been made without covering the meniscus and edges.

Finally, it is convenient to have the original, constant layer peak as a reference at fixed position. In order to demonstrate that the small peak 1′ is indeed the film peak, a few X-ray reference measurements were performed with the meniscus covered with a copper mask. The diffraction signal then originates only from

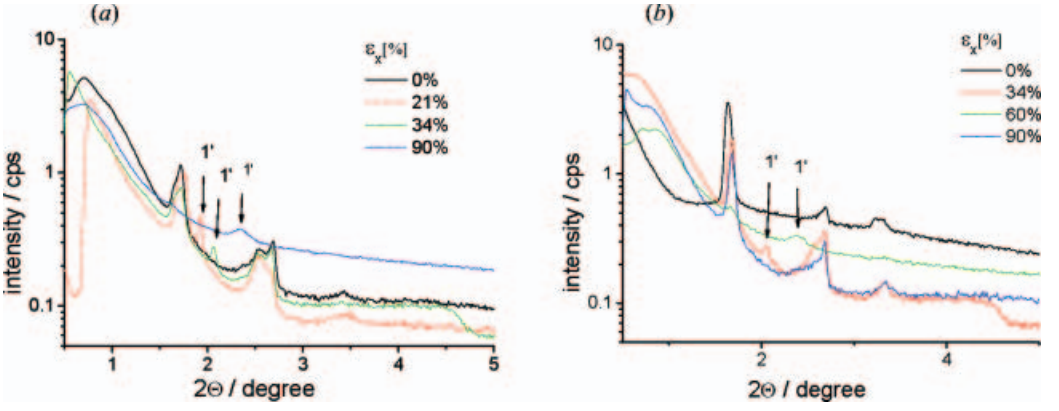

Figure 7. SAXS measurement for a free-standing smectic elastomer film at different values of deformation: (*a*) SmA phase at $T = 120°C$, (*b*) SmC* phase $T = 90°C$.

the oriented material in the free-standing film, and the bulk peaks disappear. This proves that the peaks labelled 1 and 3 in figure 6 correspond to diffraction from the meniscus or bulk material or from non-deformed, strain-free parts of the film close to the meniscus. In figure 7, one can also see that the intensities of peaks 1 and 3 reduce drastically with increasing elongation of the film, when the edges are moved progressively sideways, out of the X-ray footprint.

We now concentrate on the evaluation of the film peak labelled 1′ in figure 7. The decreasing layer thickness d can be extracted quantitatively from the shift of this peak towards larger scattering angles 2Θ with increasing strain $\Delta x/x_0$ of the film. The intensity of the scattering peak that originates from the sub-micrometer thick film is very small. It could not be identified in all films investigated, which we attribute to problems with sensitivity and adjustment of the X-ray scattering geometry. Only under optimal conditions could the scattering from the small amount of material in the film be detected in our set-up. In all cases where we have managed to find the film peak, it shows the same characteristic behaviour with increasing strain. As seen in figures 7 (*a*) and 7 (*b*), the behaviour in the SmA and SmC* phases is qualitatively the same.

Figure 8 shows the smectic layer spacing d extracted from Bragg's equation as a function of the deformation. Filled squares give the experimental results, and the solid line represents the calculated thickness change if we consider the film as incompressible isotropic material, and $\Delta d/d_0 = \Delta d_{\mathrm{film}}/d_{\mathrm{film},0}$, where d_0 is the original thickness of the smectic layers in the non-deformed sample. From the graphs, it is clear that the contraction of the film normal to the layer plane is indeed strongly correlated with the compression of the smectic layers by lateral stress, and the film thickness change is proportional, to a good approximation, to the molecular layer thickness change. We conclude that the elastic moduli for deformations parallel and perpendicular to the smectic layers have comparable values, i.e. the enthalpic part of the compression modulus for the material investigated here is negligible with respect to entropy elasticity. This result is in quantitative agreement with the optical reflectometry data discussed in the previous section.

The width of the 1′ peak of the film increases with increasing strain, while the integral intensity of this peak is conserved. This indicates that, as expected, the strain is not completely uniform in the film plane, and with increasing strain, the distribution width of the strain in the film increases.

4. Conclusions and discussion

The influence of uniaxial strain in the smectic layer plane on optical thickness, and on the smectic layer structure of the smectic LCE films crosslinked in the smectic A phase, has been studied using optical reflectometry and small angle X-ray scattering. The X-ray measurements confirm that the smectic LCE films have a lamellar structure with smectic layers parallel to the film surface. Optical reflectometry shows that in the investigated smectic LCE, stretching parallel to the smectic layers leads to a decreasing optical thickness of the film. It has been shown that this is equivalent to the physical shrinkage of the film thickness at approximately constant refractive index. The strain dependence of the film thickness found from optical reflectometry is, within experimental uncertainty, close to the

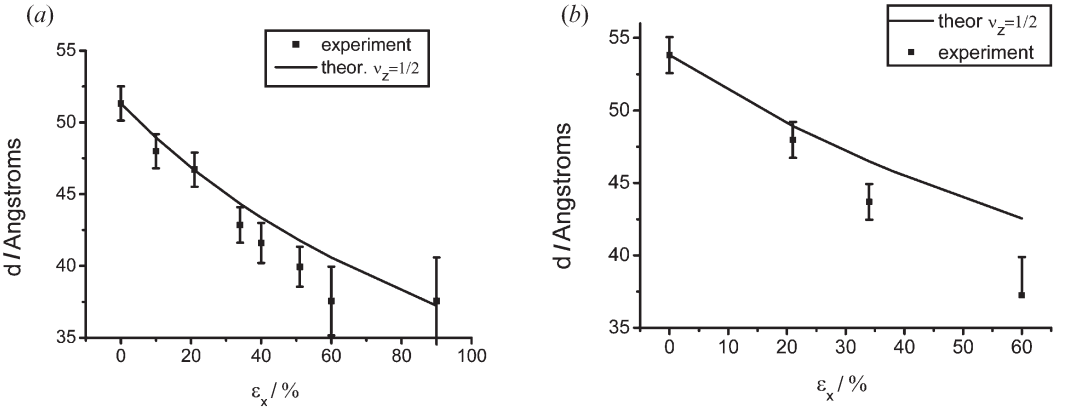

Figure 8. Dependence of the smectic layer spacing on strain; squares represent experimental values obtained from SAXS measurements of the free-standing smectic elastomer films: (*a*) SmA phase at $T = 120^{\circ}$C, (*b*) SmC* phase at $T = 90^{\circ}$C. The solid line represents the relative thickness as a function of strain calculated for an isotropic material (Poisson ratio $\nu = 1/2$).

theoretical dependence for isotropic incompressible rubbers. Much more important are the results of SAXS measurements which confirm that the change of film thickness under uniaxial stress in the smectic layer plane originates from a decreasing smectic layer spacing in the SmA and SmC* phases. Such an effect has not been previously observed for smectic A elastomers. It is the first observation that the molecular layer structure in an LCE can be deformed elastically and reversibly by mechanical forces.

Thickness variations obtained from X-ray measurements and optical reflectometry are in quantitative agreement. This confirms that the optical reflectometry method is sufficiently precise to study the deformations of thin LCEs films; that the assumption of a constant refractive index is justified; and that consequently the optical path change corresponds to an actual film thickness change. The dependence of the smectic layer thickness upon strain in x is also in good agreement with the model of an isotropic, incompressible body where molecular lattice dimensions are scaled proportionally to the macroscopic sample dimensions. The Poisson ratio for the given material is close to ½, i.e. the elastic moduli in the smectic layer plane and perpendicular to it have comparable values. The smectic layer structure hardly influences the elastic behaviour. This is in agreement with earlier observations that the elastic moduli are nearly equal in the smectic A and isotropic phases. The coupling of the elastic network with the mesogens, on the other hand, is sufficiently strong to change the smectic layer thickness.

One possible explanation involves the de Vries model for the SmA phase in the elastomer material. The de Vries diffuse cone model considers that the mean square of the molecular tilt is not zero. The difference to a smectic C phase is that the tilt azimuth is not correlated within the layers or between adjacent layers [9, 32–34]. Some mesogenic materials show only a small change of the smectic layer thickness near the smectic A–C transition (so called non-layer-shrinking smectics). This behaviour is often taken as evidence for a de Vries-type smectic A to smectic C transition [32, 33]. In smectic elastomers formed by such a material, the tilt angle of the mesogenic units can easily adapt to the deformation of the LCE film and a compression of the mesogen layers could be associated with a slight variation of the polar tilt angle. Alternatively, it is possible that during compression of the elastomers studied here, normal to the smectic layers, neighbouring layers interpenetrate mutually. Since the mesogen layers are separated by non-mesogenic, structureless siloxane layers, this may require much lower energy than in conventional low molar mass smectics, and the layer compression modulus may therefore be comparably small. The X-ray measurements cannot distinguish directly which of the two explanations is correct, while they demonstrate unambiguously that the smectic layers can be compressed reversibly by up to 30% by stretching the samples.

Acknowledgement

This study was supported by the Deutsche Forschungsgemeinschaft within project STA 425/14.

References

[1] R. Köhler, R. Stannarius, C. Tolksdorf, R. Zentel. *Appl. Phys. A*, **80**, 381 (2005).
[2] W. Lehmann, H. Skupin, C. Tolksdorf, E. Gebhard, R. Zentel, P. Krüger, M. Lösche, F. Kremer. *Nature*, **410**, 447 (2001).
[3] W. Gleim, H. Finkelmann. In *Side Chain Liquid Crystalline Polymers*, C.B. McArdle (Ed.), Blackie and Son, Glasgow (1989); H. Finkelmann. In *Liquid Crystallinity in Polymers*, A. Ciferri (Ed.), VCH, Weinheim (1991).
[4] E. Nishikawa, H. Finkelmann. *Macromol. Chem. Phys.*, **200**, 312 (1999).
[5] E. Nishikawa, H. Finkelmann, H.R. Brand. *Macromol.rapid Commun.*, **18**, 65 (1997).
[6] R. Stannarius, R. Köhler, M. Rössle, R. Zentel. *Liq. Cryst.*, **31**, 895 (2004).
[7] H. Schüring, R. Stannarius, C. Tolksdorf, R. Zentel. *Macromolecules*, **34**, 3962 (2001).
[8] R. Stannarius, R. Köhler, U. Dietrich, M. Lösche, C. Tolksdorf, R. Zentel. *Phys. Rev. E*, **65**, 041707 (2002).
[9] M. Rössle, L. Braun, D. Schollmeyer, R. Zentel, J.P.F. Lagerwall, F. Giesselmann, R. Stannarius, Unpublished results.
[10] E.M. Terentjev. *J. Phys. Cond. Mat.*, **11**, R239 (1999).
[11] I. Kundler, E. Nishikawa, H. Finkelmann. *Macromol. Symp.*, **117**, 11 (1997).
[12] R. Zentel. *Angew. Chem. adv. Mater.*, **101**, 1437 (1989).
[13] F.J.J. Davis. *J. mater. Chem.*, **3**, 551 (1993).
[14] S.M. Kelly. *Liq. Cryst.*, **24**, 71 (1998).
[15] G.C.L. Wong, W.H. de Jeu, H. Shao, K.S. Liang, R. Zentel. *Nature*, **389**, 576 (1997).
[16] T. Eckert, H. Finkelmann. *Macromol. rapid Commun.*, **17**, 767 (1996).
[17] K. Semmler, H. Finkelmann. *Macromol.Chem.Phys.*, **196**, 3197 (1995).
[18] H. Wermter, H. Finkelmann. *e-polymers*, p. 13 (2001).
[19] H. Finkelmann, E. Nishikawa, G.G. Pereira, M. Warner. *Phys. Rev. Lett.*, **87**, 015501 (2001).
[20] S.M. Clarke, A.R. Tajbakhsh, E.M. Terentjev, M. Warner. *Phys. Rev. Lett.*, **86**, 4044 (2001).
[21] Y. Mao, M. Warner. *Phys. Rev. Lett.*, **86**, 5309 (2001).
[22] M. Warner, E.M. Terentjev, R.B. Meyer, Y. Mao. *Phys. Rev. Lett.*, **85**, 2320 (2000).
[23] B. Taheri, A.F. Munoz, P. Palffy-Muhoray, R. Twieg. *Mol. Cryst. liq. Cryst.*, **358**, 73 (2001).

[24] H. Finkelmann, S.T. Kim, A. Munoz, P. Palffy-Muhoray, B. Taheri. *Adv. Mater.*, **13**, 1069 (2001).
[25] M. Brehmer, et al. *Macromol. Chem. Phys.*, **195**, 1891 (1994).
[26] M. Brehmer, R. Zentel. *Macromol. Chem. rapid Commun.*, **16**, 659 (1995).
[27] I. Benné, K. Semmler, H. Finkelmann. *Macromolecules*, **28**, 1854 (1995).
[28] M. Brehmer, et al. *Liq. Cryst.*, **21**, 589 (1996).
[29] E. Gebhard, R. Zentel. *Macromol. Chem. Phys.*, **201**, 902 (2000).
[30] R. Stannarius, H. Schüring, C. Tolksdorf, R. Zentel. *Mol. Cryst. Liq. Cryst.*, **364**, 305 (2001).
[31] R. Köhler, et al. *Proc. SPIE*, **4759**, 483 (2002).
[32] M. Rössle, R. Zentel, J.P.F. Lagerwall, F. Giesselmann. *Liq. Cryst.*, **31**, 883 (2004).
[33] C.C. Huang, S.T. Wang, X.F. Han, A. Cady, R. Pindak, W. Caliebe, K. Ema, K. Takekoshi, H. Yao. *Phys. Rev. E*, **69**, 041702 (2004).
[34] L. Naji, R. Stannarius, S. Grande, M. Rössle, R. Zentel. Unpublished results.